

Optimized Inhibitors of Soluble Epoxide Hydrolase Improve in Vitro Target Residence Time and in Vivo Efficacy

Kin Sing Stephen Lee,[†] Jun-Yan Liu,[†] Karen M. Wagner,[†] Svetlana Pakhomova,^{||} Hua Dong,[†] Christophe Morisseau,[†] Samuel H. Fu,[†] Jun Yang,[†] Peng Wang,^{†,§} Arzu Ulu,[†] Christina A. Mate,[†] Long V. Nguyen,[†] Sung Hee Hwang,[†] Matthew L. Edin,[⊥] Alexandria A. Mara,[⊥] Heike Wulff,[‡] Marcia E. Newcomer,^{||} Darryl C. Zeldin,[⊥] and Bruce D. Hammock^{*,†}

[†]Department of Entomology and Nematology, UCD Comprehensive Cancer Center, University of California Davis, One Shields Avenue, Davis, California 95616, United States

[‡]Department of Pharmacology, University of California Davis, Davis, California 95616, United States

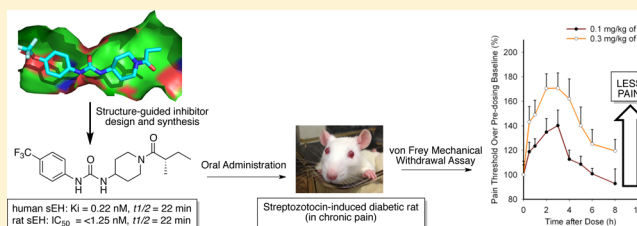
[§]Department of Applied Chemistry, China Agricultural University, Beijing 100193, People's Republic of China

^{||}Department of Biological Sciences, Louisiana State University, Baton Rouge, Louisiana 70803, United States

[⊥]Division of Intramural Research, National Institute of Environmental Health Sciences, National Institutes of Health, Research Triangle Park, North Carolina 27709, United States

S Supporting Information

ABSTRACT: Diabetes is affecting the life of millions of people. A large proportion of diabetic patients suffer from severe complications such as neuropathic pain, and current treatments for these complications have deleterious side effects. Thus, alternate therapeutic strategies are needed. Recently, the elevation of epoxy-fatty acids through inhibition of soluble epoxide hydrolase (sEH) was shown to reduce diabetic neuropathic pain in rodents. In this report, we describe a series of newly synthesized sEH inhibitors with at least 5-fold higher potency and doubled residence time inside both the human and rodent sEH enzyme than previously reported inhibitors. These inhibitors also have better physical properties and optimized pharmacokinetic profiles. The optimized inhibitor selected from this new series displayed improved efficacy of almost 10-fold in relieving pain perception in diabetic neuropathic rats as compared to the approved drug, gabapentin, and previously published sEH inhibitors. Therefore, these new sEH inhibitors could be an attractive alternative to treat diabetic neuropathy in humans.



INTRODUCTION

A recent survey from the Centers for Disease Control and Prevention indicates that diabetes affects 25.8 million people in the United States which is 8.3% of the U.S. population.¹ Most diabetic patients will ultimately develop kidney failure, hypertension, and/or suffer stroke. In addition, about two-thirds of diabetic patients will develop peripheral neuropathy.^{2,3} People suffering from diabetic neuropathic pain experience spontaneous pain (pain sensation in the absence of stimulation), hyperalgesia (increased pain sensation to painful stimuli), and allodynia (pain sensation to innocuous stimuli), which greatly affect their quality of life. Hyperglycemia has been suggested to be the initiating cause of peripheral nerve fiber degeneration, which results in pain.⁴ However, aggressive glycemic control can only control the progression of neuronal degeneration but not reverse the neuropathy.⁴ Current treatments of diabetic neuropathy include tricyclic antidepressants, anticonvulsants, selective serotonin reuptake inhibitors, and opioids, however they often have side effects that limit their use.⁵ Therefore, an alternative therapy with no or greatly

reduced side effects is still imperative for these patients often suffering multiple comorbid conditions.

Epoxy fatty acids (EpFAs), formed by cytochrome P450 (CYP450) from polyunsaturated fatty acids, are important lipid mediators.⁶ Epoxy-eicosatrienoic acids (EETs), epoxy-eicosatetraenoic acids (EpETEs), and epoxy-docosapentaenoic acids (EpDPEs), from arachidonic acid, eicosapentaenoic acid, and docosahexaenoic acid, respectively, have analgesic properties in inflammatory pain models.^{7,8} Although these EpFAs are very potent lipid mediators, they are rapidly metabolized by soluble epoxide hydrolase (sEH EC 3.3.2.10) to their corresponding 1,2-diols and to a lesser extent by other enzymes in vivo.⁹ The in vivo biological activities of these natural chemical mediators appear limited by their rapid degradation. Stabilization of EpFAs through inhibition of sEH has shown anti-inflammatory, antihypertensive, and analgesic effects. Recent studies also indicate that sEH inhibition is analgesic in chronic diabetic

Received: May 5, 2014

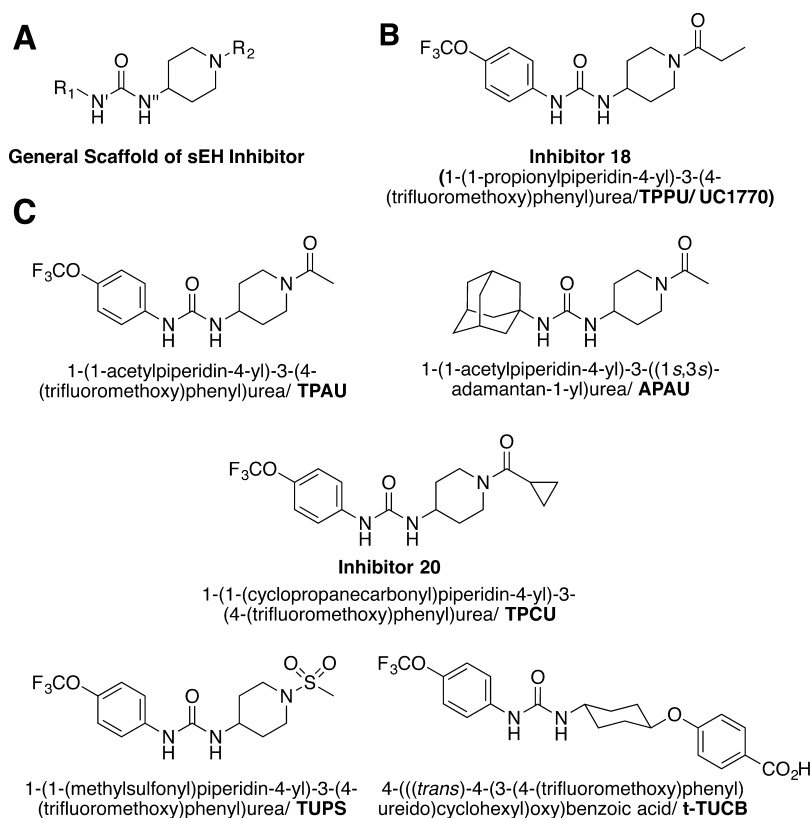


Figure 1. (A) The general scaffold of sEH inhibitors used in this report. (B) The structure of inhibitor 18 (TPPU/UC1770). (C) The name structures of previously published inhibitors.

neuropathic pain in animal models. In fact, it is more efficacious than gabapentin, a clinically approved drug for this condition.^{10,11} In nonmodel species, sEH inhibitors have reduced the inflammatory and devastating neuropathic pain in laminitis horses,¹² reduced blood pressure in forearm blood flow studies in man,¹³ and reduced neuropathic pain in human diabetics (www.sphaerapharma.com). Thus, sEH is a potentially important pharmaceutical target.^{6,8,9,12,14–20}

Over the years, several groups have reported the synthesis and evaluation of sEH inhibitors with different central pharmacophores with potency varying from micromolar to nanomolar ranges.^{21–27} The 1,3-disubstituted urea is one of the more potent central pharmacophores being used to inhibit sEH because the urea forms tight hydrogen bonds with the active residue Asp335 and the chemistry is easily accessible.^{21,23,28–30} The physical properties of many of the most potent compounds are generally poor. Efforts to improve physical properties including water solubility, hydrophilicity, decreased clogP, and lowered melting point of sEH inhibitors have generally resulted in a decrease in potency and less desirable pharmacokinetics. These physical properties can also result in poor absorption and inferior pharmacokinetic properties and can demand heroic formulation.^{26,30–32} Therefore, it is necessary to further optimize the structures of the inhibitors and improve the oral bioavailability of the sEH inhibitors carrying a 1,3-disubstituted urea as a central pharmacophores.

Recent reports in drug discovery suggest that the residence time of a drug in its target is an important parameter to predict in vivo drug efficacy.³³ Residence time is defined as the duration of time which the target, either enzyme or receptor, is occupied by the ligand.³³ The traditional IC₅₀ and K_i or K_d is determined in a closed in vitro system in which the

concentrations of the ligand and the target are constant. However, an in vivo system is an open system, thus the target is exposed to a varying concentration of ligand after dosing because of circulation, metabolism, and excretion. Therefore, drug efficacy is no longer correlated with the in vitro potency (IC₅₀ or K_i) that is determined in a closed system but rather depends on the duration the target is occupied by the ligand. This residence time can be calculated from the reciprocal of the dissociation rate constant (*k*_{off}) of the target–ligand complex.

In this report, inhibitors with improved potency have been designed and synthesized based on the *holo*-structure of the recombinant human sEH with published sEH inhibitor: TPPU (UC1770)²³ (Figure 1B). Their residence times have been determined and their in vivo efficacies have been tested in a diabetic neuropathic pain model.

RESULTS AND DISCUSSION

Inhibitor Design and Synthesis. Piperidyl-urea inhibitors of sEH were first described in 2006 and have the general scaffold shown in Figure 1A.^{23,32} It has been demonstrated that large amide substituents at R₂ improve the potency of the sEH inhibitors (Figure 1A).²³ However, sEH inhibitors with large amide substituents at R₂ (Figure 1A) exhibit poor pharmacokinetic profiles in dogs.³⁴ To further improve both the potency and pharmacokinetic profiles of the sEH inhibitors, we started with a published inhibitor having a small substituent at R₂: TPPU (inhibitor 18) (Figure 1B), which resulted in good potency and a good pharmacokinetic profile. Because of the favorable properties of inhibitor 18, an X-ray structure of human sEH with inhibitor 18 was obtained and used to predict structural modifications of inhibitors leading to improved

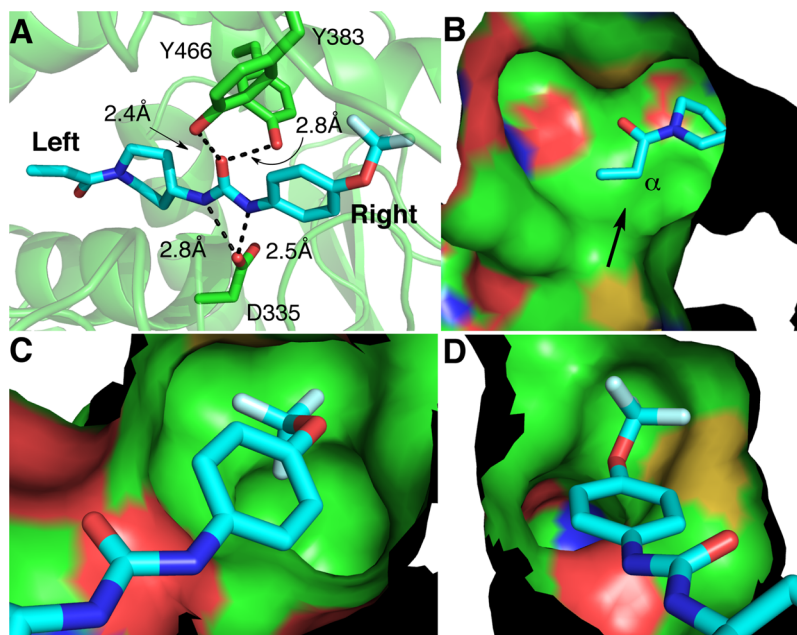


Figure 2. (A) Holo-crystal structure of *human* sEH (green) with inhibitor **18** (TPPU) (cyan) (PDB code: 4OD0). (B) The left side of the tunnel of *human* sEH with inhibitor **18** (cyan). The arrow indicated the valley of the left side of the tunnel for potential additional binding for new inhibitors. (C,D) The right binding pocket of *human* sEH with UC1770 from the view of the front and back (cyan). The graphics were prepared by the PyMOL Molecular Graphics System, version 1.3 edu, Schrodinger, LCC.

potency and properties. The X-ray structure indicates that there is a small secondary binding site (valley) next to the α -carbon of the amide of inhibitor **18** (Figure 2A,B), which can provide additional binding possibilities. We therefore hypothesized that the potency of the inhibitors could be significantly improved by incorporating a small hydrophobic substituent at the α -carbon of the amide (Figure 2B). In addition, the 4-trifluoromethoxyphenyl- group on the urea of inhibitor **18** fits closely to the “right side” of the binding pocket with only a little room for additional binding (Figure 2C,D). Thus, only substituents which are similar to the size of the 4-trifluoromethoxyphenyl- group were used for inhibitor optimization. On the basis of these findings, a series of 30 piperidyl-ureas was made using four different methods described previously.²³ These methods with slight modifications are summarized in Scheme 1 (detailed synthetic procedures are provided in the Supporting Information).

Optimization of the Potency (K_i) of sEH Inhibitors. A new series of sEH inhibitors was synthesized with various substituents at R_2 on the amide (Table 1) while maintaining R_1 as a 4-trifluoromethylphenyl- group. In general, as the size of the substituent increases, the potency of the inhibitors against *human* sEH increases. As we hypothesized, addition of a methyl- group on the α -carbon of the amide (Figure 1A) greatly improves the potency by almost 5-fold (inhibitors **2** vs **4** and inhibitors **3** vs **6**). Interestingly, replacing the isopropyl- (**4**) with cyclopropyl- group (**5**) also results in a slight increase in potency, an increase in water solubility, and a decrease in melting point. The elongation of the aliphatic chain by one carbon (inhibitors **2** vs **3**) slightly enhances (30%) the potency (Table 1). To investigate whether the enhanced potency of inhibitor **6** is stereospecific, we tested the corresponding *S*-isomer (inhibitor **7**), which is 2-fold more potent than its racemic mixture (Table 1), suggesting that the *R*-isomer is less active. The related inhibitor **8** is less potent than inhibitors **6** and **7**, which indicates that the addition of methyl- group not

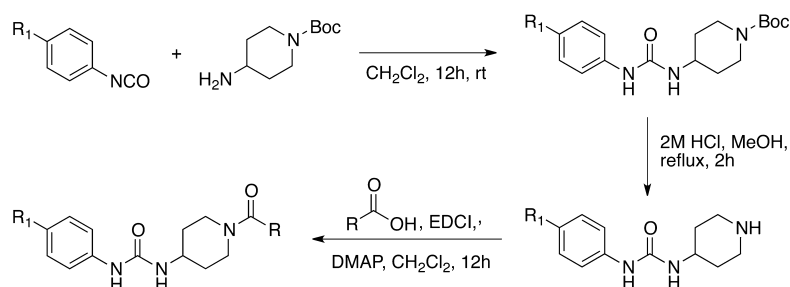
only is stereospecific but is also regiospecific. An X-ray structure of *human* sEH with inhibitor **4** shows that the methyl- group on the α -carbon of the amide of inhibitor **4** effectively fits into the additional binding site on the right side of the binding pocket (Figure 3). This additional binding site was predicted from the crystal structure of *human* sEH with inhibitor **18** (Figure 2B).

Although the addition of an alkyl group enhances the potency of this series of sEH inhibitors, their metabolic stability will likely decrease because the added alkyl group at the α -position is expected to be metabolized faster. This also increases the lipophilicity of the inhibitors, which may increase their affinity to CYP450 enzymes that are responsible for drug oxidation.³⁵ Because fluoride replacement is known to decrease metabolism,³⁶ we synthesized inhibitor **9**,³⁶ and it shows potency similar to inhibitor **8**. The size of the CF_3 - group is similar to the size of the isopropyl-, group and the potency of inhibitor **9** is maintained. This could provide an approach to increase the stability of the inhibitors without hampering the potency of the inhibitors.

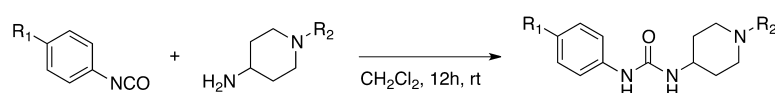
We then further optimized the potency of sEH inhibitors by modifying the substituent at R_1 while maintaining the 2-methyl butanoyl group at R_2 (Table 2). The binding pocket is very hydrophobic (Supporting Information, Figure S2) with limited space (Figure 2C,D). Therefore, the size of R_1 was modified slightly in order to test if increasing the hydrophobic surface of the inhibitors could enhance their potency. Consequently, inhibitors **11** and **12** were synthesized (Table 2). The result indicates that there is steric hindrance within the right binding pocket (Figure 2C,D). Thus, the potency of the inhibitor dropped when the size of the substituent at R_1 (Figure 1A) was increased from a 4-*iso*-propylphenyl group to a 4-*tert*-butylphenyl- group (inhibitors **11** and **12**) (Table 2). It is interesting that the inhibitor **6**, which has CF_3 - group in place of an *iso*-propyl- and *tert*-butyl- group,³⁷ is more potent as an inhibitor when compared to inhibitors **11** and **12**. To

Scheme 1. Synthetic Schemes for sEH Inhibitors Synthesis

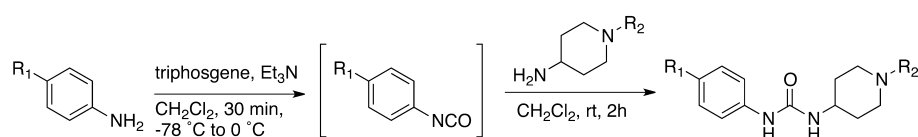
Synthetic Pathway 1



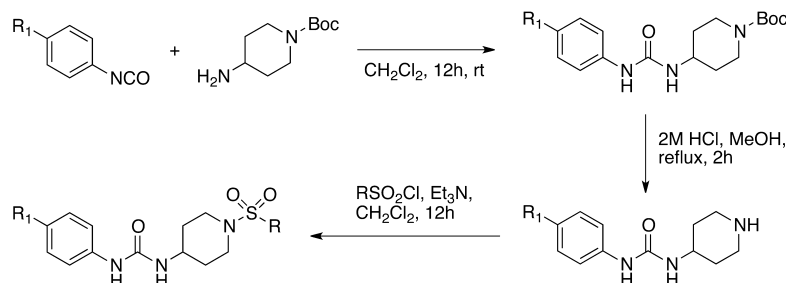
Synthetic Pathway 2



Synthetic Pathway 3



Synthetic Pathway 4

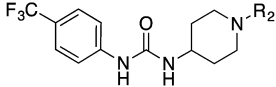
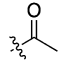
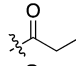
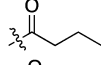
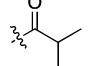
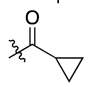
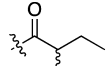
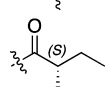
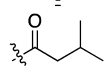
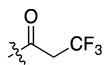
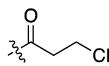


investigate whether the enhanced potency of inhibitor **6** is due to fluorine induced interactions or better occupancy of the binding pocket, the 4-*t*-butylphenyl- group of inhibitor **12** was replaced by its isostere: a 4-heptafluoro-*iso*-propyl-phenyl group at R₁ of inhibitor **13**.³⁷ This compound is 20-fold more potent than inhibitor **6**, which indicates that the fluorine induced interactions in the left binding pocket are very strong (Table 2). These data suggest that the left side of the binding pocket is likely fluorophilic. Interestingly, replacement of the 4-trifluoromethylphenyl- at R₁ of inhibitor **6** by a 4-trifluoromethoxyphenyl- group (inhibitor **14**) did not alter potency, but the replacement improved solubility by 10-fold (Table 1). Furthermore, inhibitors with a cycloalkyl- group at R₁ were synthesized, and the addition of carbon atoms (inhibitor **15** to **17**) enhances the binding toward human sEH by more than 4 times (Table 2) and placement of cycloalkyl- group at R₁ greatly enhances their solubility.

It has been reported that inhibitors with 4-trifluoromethoxyphenyl- at R₁ are more potent than inhibitors with 4-trifluoromethylphenyl- at R₁ and have better physical properties.²³ To investigate whether such substitution could enhance the potency of the inhibitors and improve physical properties in general,³⁸ a series of inhibitors with 4-trifluoromethylphenyl group at R₁ was replaced with a 4-trifluoromethoxyphenyl- group (Figure 1A). The results suggest that substitution of 4-

trifluoromethylphenyl- with 4-trifluoromethoxyphenyl- enhances the potency of certain inhibitors (**2** vs **18** and **4** vs **19** in Tables 1 and 3), but there is no substantial improvement with inhibitors with the 2-methyl butanoyl group at R₂ (**6** vs **14** and **7** vs **21** in Table 1–3) or the cyclopropyl group at R₂ (**5** Vs **20**). This may be due to the possibility of different binding orientations than the one shown in Figure 2A and in previous crystallography.³⁹ Therefore, two inhibitors which are structurally similar to **21** but with urea substituted by the amide (**22** and **23**) were synthesized. In general, structure–activity relationships developed with the urea central pharmacophore are predictive of enzyme inhibition with amide and carbamate. Both inhibitors **22** and **23** are less potent than their corresponding urea (**21**) (Table 3). Compound **22**, which has amide nitrogen (N''H) on the piperidine side (Figure 1A), is far less potent than the amide **23**, which has an amide nitrogen (N'H) on the R₁ side (Figure 1A) (Table 2). It indicates that the urea N'H–Asp(O) interaction is stronger than the urea N''H–Asp(O) interaction by 5.7 kJ mol^{−1}, calculated based on the K_i of both inhibitors. This result is consistent with the crystal structure where the distance between urea N'H and Asp(O) is shorter than the distance between urea N''H and Asp(O) hydrogen bonding (Figure 2A). In some cases, the placement of 4-trifluoromethoxyphenyl- at R₁ (Figure 1A) enhances the potency of sEH inhibitors, but in

Table 1. Physical Properties and Potency of sEH Inhibitors against Human sEH (Modification of R₂)^e

Inhibitor	R ₂		Physical Properties			Human sEH
			Solubility (ug/mL) ^a	Melting Point (°C)	elogP ^c	K _i (nM) ^d
1	R ₂ :		8.95	244.0-248.7 (246.4)	2.74	14.6±1.70
2			N.D. ^b	224.0-228.0 (226)	N.D. ^b	2.96±0.60
3			N.D. ^b	192.3-197.6 (193.6)	N.D. ^b	2.23±0.71
4			7.20	234.1-235.4 (234.9)	3.37	0.66±0.10
5			19.7	193.4-194.2 (193.7)	3.18	0.49±0.08
6			2.63	225.2-226.3 (225.9)	3.83	0.37±0.04
7			9.20	221.3-225.6 (221.6)	3.84	0.22±0.04
8			N.D. ^b	220-223 (221.5)	3.86	0.49±0.12
9			3.22	209.2-210.7 (210.3)	3.99	0.43±0.06
10			N.D. ^b	198.0-202.3 (199.6)	3.66	1.2±0.1

^aSolubility was measured with sodium phosphate buffer (0.1 M, pH 7.4) according to the method described by Tsai et al. and described in detail in Supporting Information.³⁴ ^bN.D. means "not determined". ^celogP was determined by HPLC method calibrated with elogP of six selected inhibitors determined by the shake-flask method (Supporting Information, Figure S3). ^dK_i was determined by FRET-based displacement assay described by Lee et al.³⁸ The results are the average of duplicates with ± SEM. ^eAbbreviation: elogP stands for experimental Log P.

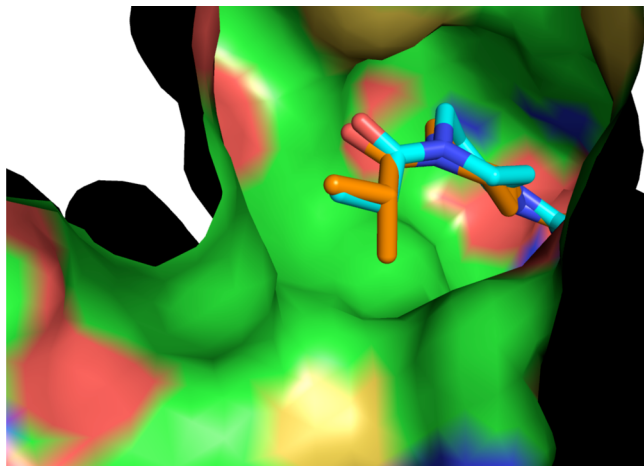


Figure 3. Overlay structures of human sEH with inhibitor 18 (cyan) and inhibitor 4 (orange). This figure suggests that the design principle is valid and the methyl- group at α -position of the amide provides extra binding toward the valley of the left binding pocket. The graphics were prepared by the PyMOL Molecular Graphics System, version 1.3 edu, Schrodinger, LCC.

all cases, this substitution decreases the melting point and improves the solubility of the inhibitors (Tables 1–3). These improvements of physical properties ease the drug formulation process.

It was reported that replacement of amide with sulfonamide at R₂ was shown to enhance the potency of the inhibitors. However, such observations were based on very few comparisons.^{23,34} Therefore, a new series of inhibitors with a different sulfonamide at R₂ was synthesized for a more detailed study (Table 4). In general, the potency of the inhibitors increases with the size of R₂ (7-fold better potency from a methyl 25 to a butyl 31). However, unlike the inhibitor with an amide at R₂ (Table 1), the placement of an *iso*-propylsulfonamide at R₂ (29 vs 26) does not significantly enhance the potency against human sEH. This is probably because the sulfonamide exists as a tetrahedron while amide is trigonal planar and the S(O)₂–C bond is at least 0.28 Å longer than the C(O)–C bond.⁴⁰ These data further indicate that the enhanced potency of the methyl substitution at the α -position of the amide is structurally specific. Overall, unlike previously reported, the inhibitors with a sulfonamide at R₂ are less potent than the inhibitors with amides at R₂. In addition, the physical properties (solubility and melting point) of inhibitors with a sulfonamide at R₂ are generally poor as compared to inhibitors with amides at R₂.

Here, we have identified several structural changes that can significantly enhance the potency and improve the physical properties of the inhibitors. We have also demonstrated that the sulfonamide at R₂ is less attractive than the corresponding amide.

Table 2. Physical Properties and Potency of sEH Inhibitors against Human sEH (Modification of R₁)^e

Inhibitor	R ₁	Physical Properties			Human sEH
		Solubility (ug/mL) ^a	Melting Point (°C)	eLogP ^c	K _i (nM) ^d
6		2.60	225.2-226.3 (225.9)	3.83	0.37±0.04
11		2.60	174.0-174.9 (174.5)	4.21	1.17±0.27
12		0.02	213.2-216.6 (214.3)	5.12	2.44±0.30
13		0.17	182.2-183.2 (182.8)	4.96	0.02±0.01
14		22.5	170.9-171.6 (171.3)	3.98	0.36±0.09
15		923	127.7-130.5 (128.5)	N.D. ^b	4.23±0.07
16		278	122.4-124.2 (122.9)	N.D. ^b	0.99±0.06
17		39.5	149.8-150.8 (150.4)	N.D. ^b	0.23±0.07

^aSolubility was measured with sodium phosphate buffer (0.1 M, pH 7.4) according to the method described by Tsai et al. and described in detail in Supporting Information.³⁴ ^bN.D. means "not determined". ^ceLogP was determined by HPLC method calibrated with eLogP of six selected inhibitors determined by the shake-flask method (Supporting Information, Figure S3). ^dK_i was determined by FRET-based displacement assay described by Lee et al.³⁸ The results are the average of duplicates with ± SEM. ^eAbbreviation: eLogP stands for experimental Log P.

New sEH Inhibitors Have Improved Dissociation Rate Constants (*k*_{off}) against Human sEH. Recent studies have suggested that *k*_{off}, a kinetic parameter on enzyme inhibition, from the enzyme is a better indicator for in vivo potency than *K_i*.³³ This is because inhibitors are only effective in blocking catalysis when the target proteins are occupied by the inhibitors. The *k*_{off} can provide more detailed information, about the duration of time the inhibitors are bound to the target enzyme (target occupancy) than the *K_i*, an equilibrium parameter on enzyme inhibition, and ultimately this translates into in vivo efficacy.⁴⁰ Therefore, a small set of new potent inhibitors together with several potent published inhibitors (Figure 1C) were selected to determine their *k*_{off} against sEH using a recently developed FRET-based assay.³⁸

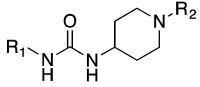
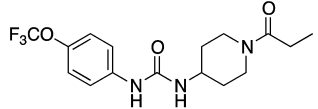
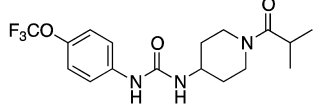
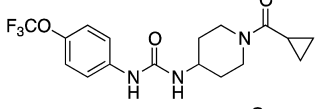
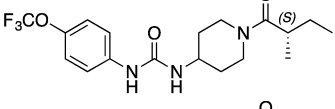
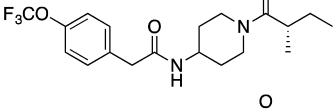
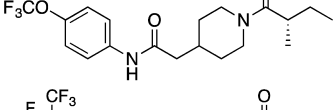
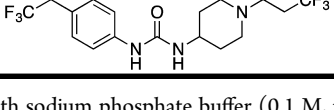
The result indicates that the *k*_{off} of inhibitors decreases with the size of R₂ increased (Table 5 and Figure 1C, inhibitor 4 < 7; TPAU < 18 (TPPU) < 19 < 21; and TUPS < 32). However, the *k*_{off} does not substantially change when the R₁ was varied among a 4-trifluoromethylphenyl- group (inhibitor 6), a 4-trifluoromethoxyphenyl- group (inhibitor 14), and a 4-isopropylphenyl- group (inhibitor 11) (Table 5). The 4-heptafluoroisopropylphenyl- group at R₁ (inhibitor 13 and inhibitor 24) significantly decreased the *k*_{off} of the inhibitors. This further supports our hypothesis that the pocket is fluorophilic and the added fluorines can induce several interactions with the nearby residues within the binding pocket. The *k*_{off}s of new inhibitors are slower overall, indicating a longer residence time in the target and have at least a 2-fold slower off rate than any of the previously published inhibitors

(Table 5 and Figure 1C, APAU, TPAU, 18 (TPPU), TUPS, t-TUCB).

To investigate relationship of *k*_{off} with *K_i* and other physical properties of the inhibitors, correlation graphs of *k*_{off} with these parameters were plotted (Supporting Information, Figure S1A). The results show no correlation (*R*² = 0.21) between the number of non-hydrogen atoms and *k*_{off}. However, there is a trend showing (*R*² = 0.52) that an increase in eLogP results in a decrease of *k*_{off} (Supporting Information, Figure S1B). This may due to the fact that the binding pocket of the human sEH is hydrophobic (Supporting Information, Figure S2). An increase of hydrophobicity of the ligand increases the lipophilic interactions with the binding pocket. Therefore, it requires higher activation energy to break up the interactions between protein and the bound inhibitors. In addition, a correlation between *K_i* and *k*_{off} was plotted (Supporting Information, Figures S1C, S1D). The plot indicates that there is a good correlation between *K_i* and *k*_{off} (*R*² = 0.88) over a wide range of potencies (from 0 to 20 nM). However, when we focused on a narrower range of potencies (from 0 to 1.4 nM), the correlation is moderate (*R*² = 0.44). Because *K_i* is a ratio of *k*_{off} over *k*_{on}, *K_i* should be inversely proportional to *k*_{off}. Therefore, the poor correlation over a moderate range *K_i* values suggests that the differences are due to the *k*_{on}. These results indicate that it is possible to specifically modulate *k*_{off} without greatly affecting *K_i*.

An Improved Pharmacokinetic Profile of New Series of sEH Inhibitors. To investigate the oral bioavailability of sEH inhibitors, we determined the pharmacokinetic profiles post oral administration. Cassette dosing was used as a

Table 3. Physical Properties and Potency of sEH Inhibitors against Human sEH (Modification of R₁)^e

Inhibitor		Physical Properties			Human sEH
		Solubility (ug/mL) ^a	Melting Point (°C)	elogP ^c	Ki (nM) ^d
18 (TPPU)		60	198.2-200.8 (199.5)	3.23	0.91±0.13
19		27.0	179.1-180.3 (179.6)	3.56	0.31±0.18
20 (TPCU)		4.6	193.4-194.2 (193.8)	3.28	0.55±0.10
21		21.3	168.0-169.3 (168.7)	3.97	0.19±0.04
22		N.D. ^b	91.2-92.6 (91.7)	N.D. ^b	111±13
23		N.D. ^b	Gel-like	N.D. ^b	11.2±0.42
24		12.3	131.8-135.8 (133.8)	4.89	<0.02

^aSolubility was measured with sodium phosphate buffer (0.1 M, pH 7.4) according to the method described by Tsai et al. and described in detail in Supporting Information.³⁴ ^bN.D. means "not determined". ^celogP was determined by HPLC method calibrated with elogP of six selected inhibitors determined by the shake-flask method (Supporting Information, Figure S3). ^dK_i was determined by FRET-based displacement assay described by Lee et al.³⁸ The results are the average of duplicates with ± SEM. ^eAbbreviation: elogP stands for experimental Log P.

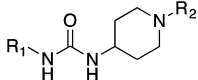
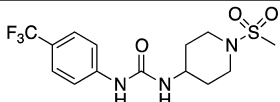
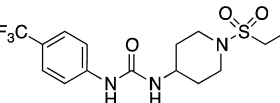
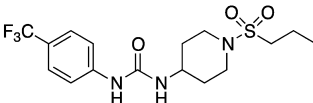
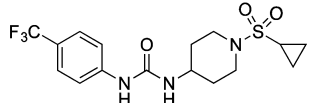
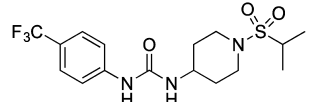
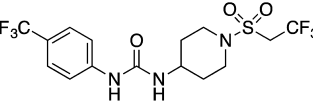
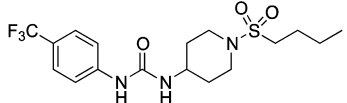
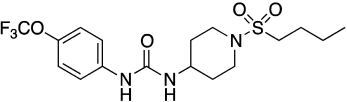
screening tool to select the compounds for more detailed study to allocate limited resources to the most promising compounds. There are cautions with cassette dosing including changes in pharmacokinetic behavior due to competition for xenobiotic metabolism. The high potency and thus low doses used in this study make this artifact less likely. A comparison of pharmacokinetic profiles of sEH inhibitors between the cassette dose and single dose carried out in nonhuman primate. The results show that there was no statistically significant difference in the pharmacokinetic behaviors between cassette and individual dosing of sEH inhibitors; therefore, cassette dosing was predictive for the compounds reported here.⁴¹

The pharmacokinetic profiles of this series of selected potent compounds also determined the effect of the position or addition of aliphatic carbons on the inhibitors. In general, the results indicate that the sEH inhibitors with a 4-trifluoromethylphenyl- group or a 4-trifluoromethoxyphenyl- group at R₁ (Figure 1A) have good drug exposure levels based on the area under the curve of the pharmacokinetic kinetic profile (PK-AUC) after oral administration (Table 6). As we replaced the 4-trifluoromethylphenyl- group or 4-trifluoromethoxyphenyl- group at R₁ with a 4-isopropylphenyl- group (inhibitors **6** or **14** vs **11**), the potency of inhibitor **14** decreases (Table 2). As we anticipated, the pharmacokinetic T_{1/2} (PK-T_{1/2}) and oral

drug exposure level estimated by PK-AUC also decreases (Table 6). Further replacement of the phenyl group at R₁ with a cycloalkyl- group (inhibitors **16** and **17**) greatly decreases the oral drug exposure level (Table 6, Supporting Information, Figures S6, S8, and S9). It is likely that each addition of an aliphatic carbon renders the molecule more susceptible to metabolism by CYP450 enzymes.⁴² Such a phenomenon was also observed as the alkyl chain length varied at R₂. As we hypothesized, the PK-T_{1/2} of the inhibitors also decrease when the alkyl chain length at R₂ of the amide and sulfonamide series increases (Table 6 for amide inhibitors, **18**, **19**, and **21**; for sulfonamide inhibitors, **25** and **TUPS** (Figure 1C) vs **31** and **32**). The result also show that the PK-AUC estimated drug exposure levels of the sulfonamide inhibitors **31** and **32** are, in general, worse than the amide inhibitors (Table 6).

We then synthesized inhibitors **9** and **24** in order to study whether the addition of fluorine could enhance the stability of our inhibitors as has been previously suggested.³⁶ The replacement of a terminal methyl group with a CF₃- group at the R₂ of the amide inhibitors (inhibitors **9** vs **TPPU** and **24** vs **13**) not only improves the PK-T_{1/2} of the inhibitors but also increases their oral drug exposure levels (Table 6). A similar result was obtained with the sulfonamide inhibitor. Inhibitor **30** shows at least a 20-fold better bioavailability based on oral PK-

Table 4. Physical Properties and Potency of sEH Inhibitors against Human sEH (Modification of R₁ and R₂ with sulfonamide at R₂)^e

Inhibitor		Physical Properties			Human sEH
		Sol. (ug/mL) ^a	Melting Point (°C)	elogP ^c	Ki (nM) ^d
25		0.67	256.8-260.1 (258.5)	2.94	7.16±0.42
26		N.D. ^b	248.0-252.5 (250.3)	3.08	1.74±0.13
27		N.D. ^b	241.5-242.6 (242.0)	3.39	1.47±0.10
28		N.D. ^b	261.8-262.6 (262.2)	3.39	1.22±0.01
29		N.D. ^b	235.6-237.2 (236.4)	3.39	1.17±0.07
30		N.D. ^b	257.6-261.0 (259.3)	3.42	1.79±0.43
31		0.08	230.4-231.1 (230.8)	3.95	0.98±0.19
32		0.60	224.0-225.2 (224.6)	4.13	0.44±0.11

^aSolubility was measured with sodium phosphate buffer (0.1 M, pH 7.4) according to the method described by Tsai et al. and described in detail in Supporting Information.³⁴ ^bN.D. means "not determined". ^celogP was determined by HPLC method calibrated with elogP of six selected inhibitors determined by the shake-flask method (Supporting Information, Figure S3). ^dK_i was determined by FRET-based displacement assay described by Lee et al.³⁸ The results are the average of duplicates with ± SEM. ^eAbbreviation: Sol. stands for Solubility; elogP stands for experimental Log P.

Table 5. Study in Vitro Target Occupancy (*k*_{off}) of Selected sEH Inhibitors against Human sEH

entry	inhibitor	<i>k</i> _{off} (× 10 ⁻⁴ s ⁻¹) ^a	<i>t</i> _{1/2} (min) ^b	entry	inhibitor	<i>k</i> _{off} (× 10 ⁻⁴ s ⁻¹) ^a	<i>t</i> _{1/2} (min) ^b
1	APAU	19.2 ± 0.70	6.03 ± 0.2	11	17	3.51 ± 0.20	33.0 ± 1.9
2	18 (TPPU)	10.5 ± 0.20	11.0 ± 0.2	12	19	6.14 ± 0.18	18.8 ± 0.6
3	4	6.57 ± 0.30	17.6 ± 0.8	13	21	5.05 ± 0.02	22.9 ± 0.1
4	5	7.91 ± 0.31	14.6 ± 0.6	14	24	4.39 ± 0.43	26.5 ± 2.6
5	6	5.76 ± 0.26	20.1 ± 0.9	15	25	23.1 ± 1.1	5.02 ± 0.3
6	7	5.19 ± 0.09	22.3 ± 0.4	16	31	10.3 ± 0.1	11.0 ± 0.1
7	9	4.75 ± 0.11	24.3 ± 0.6	17	32	8.90 ± 0.35	13.0 ± 0.5
8	11	5.79 ± 0.43	20.0 ± 1.5	18	33 (TPAU)	26.4 ± 2.30	4.40 ± 0.4
9	13	3.13 ± 0.06	37.0 ± 0.7	19	TUPS	20.0 ± 0.64	5.79 ± 0.2
10	14	5.39 ± 0.39	21.5 ± 1.6	20	t-TUCB	7.19 ± 0.36	16.1 ± 0.8

^a*k*_{off} was determined by FRET-based displacement assay described by Lee et al.³⁸ and described in detail in Supporting Information. Briefly, a preincubated human sEH–inhibitor complex (8 μM) was diluted by ×40 times by fluorescent reporter–APCU (2 μM, 0.1 M sodium phosphate, pH 7.4). The fluorescent enhancement (λ_{excit} = 280 nm, λ_{emit} = 450) was measured over time (5100 s). The results are the average of triplicates with ± SD. ^b*t*_{1/2} = ln(2)/*k*_{off} which describes the half-life of enzyme–inhibitor complex.

AUC with a substantially longer PK-*T*_{1/2} as compared to inhibitors 31 and 32 (Table 6). These data support the hypothesis that the CF₃– substitution effectively blocks

metabolism at R₂. However, addition of fluorine to the fluorinated substituents could not further enhance the stability of the inhibitors. When the inhibitors with 4-trifluoromethyl–

Table 6. Pharmacokinetic Parameters of Selected sEH Inhibitors after Oral Dosing on Mice^a

inhibitor	PK-AUC ^a (nM·h) ^b	C _{max} (nM) ^c	T _{1/2} ^b (h)	T _{max} (h) ^c
APAU ¹⁰	183	30	3	1
TUPS ¹⁸	5300	370	15	3.3
18 (TPPU)	10650	495	12.1	8
4	19650	1160	6	4
5	24630	960	17	6
6	3295	320	6	0.5
7	4940	435	5	1
9	8845	330	15.4	8
11	200	90	2	0.5
13	1600	135	4.5	2.5
14	3300	235	6	2
16	75	3	8.4	0.5
17	37	5	12	0.5
19	19500	900	9	5
21	2530	195	7.7	4
24	9600	365	18.9	8
25	4675	130	22	8
30	4270	100	25	8
31	245	30	7.4	1
32	220	65	2	1.2

^aThe mice ($n = 4$) were treated by oral dosing with a cassette of 3 to 5 compounds (0.3 mg/kg per each compounds dissolved in 20% PEG400 in oleic acid rich triglycerides). ^bThe pharmacokinetic profiles of the inhibitors were calculated by Winonlin based on the model of one compartmental analysis. ^cThe pharmacokinetic profiles of the inhibitors were calculated by Winonlin based on the model of noncompartmental analysis.

groups at R₁ were substituted by a heptafluoro-isopropyl-group (inhibitor **6** vs **13**), both the PK-T_{1/2} and bioavailability decreased (Table 6). This is probably due to the fact that the increase of *elogP* enhances the affinity toward xenobiotic metabolizing enzymes and cell membranes. These results suggest that in order to enhance the stability of the inhibitors, addition of fluorine should be carefully positioned.^{35,43}

In general, inhibitors with 4-trifluoromethylphenyl-, 4-trifluoromethoxyphenyl-, and 4-(heptafluoro-*iso*-propyl)-phenyl- groups at R₁ with amide substituents at R₂ showed good pharmacokinetic profiles. Inhibitors **16**, **17**, **31**, and **32**, although very potent, are not optimal candidates for testing in animal chronic disease models because of poor oral drug exposure levels. Our data also suggest that these inhibitors (**16**, **17**, **31**, and **32**) may not be top candidates to be optimized for human drugs. The inhibitors with a piperidyl moiety attached at N² of the urea show greatly improved oral pharmacokinetic profiles compared to inhibitors with a cyclohexyl moiety attached at N² of the urea also (Supporting Information, Figure S6).³⁰ Overall, our data suggested that several newly synthesized sEH inhibitors have an improved and optimized pharmacokinetic profile for diseases requiring chronic treatment.

New Series of sEH Inhibitors Show No Significant Nonspecific Binding toward Other Pharmacologically Important Proteins. Several of the newly synthesized sEH inhibitors selected for potency and good oral drug exposure levels were tested against a set of proteins to evaluate potential off-target side effects and nonspecific binding. Inhibitor **24** was excluded because of its relatively high *elogP* (Table 3), which was suspected to lead to high nonspecific binding. High lipophilicity is avoided when possible in medicinal chemistry

because it is associated with poor pharmacokinetic behavior and nontargeted related side effects. Although not conclusive, the pharmacokinetic studies indicated that the 4-(heptafluoro-*iso*-propyl)-phenyl group likely enhances the affinity of inhibitors toward xenobiotic metabolizing enzymes and cell membranes, potentially leading to the poor oral drug exposure of inhibitor **13** (Table 6).

It was reported that very high plasma protein binding can not only hamper the efficacy of drugs or signaling molecules but also can alter their pharmacokinetic profile.^{44,45} However, modulating plasma protein binding can help drug solubilization and drug distribution.⁴⁶ Therefore, the plasma protein binding of the selected inhibitors were measured with an assay carried out with a rapid equilibrium dialysis device based on manufacturer's protocol (Table 7). These new inhibitors

Table 7. Testing for Nonspecific Protein Binding with Selected sEH Inhibitors

inhibitor	hERG channel inhibition at 50 μ M (%) ^a	human plasma protein binding at 1 μ M (%) ^a	human CYP 2J remaining activity at 10 μ M (%) ^{b,d}	human CYP2C remaining activity at 10 μ M (%) ^{b,d}
APAU	4.5 \pm 0.5	50.0 \pm 2.0	140.0 \pm 5.0	104.0 \pm 1.0
18 (TPPU)	26.0 \pm 1.0	79.0 \pm 1.0	91.9 \pm 2.2	118.0 \pm 2.4
4	16.5 \pm 1.5	85.0 \pm 0.5	81.6 \pm 3.0	110.0 \pm 2.0
5	41.5 \pm 1.5	95.1 \pm 0.5	N.D. ^c	N.D. ^c
7	N.D. ^c	96.3 \pm 0.2	82.6 \pm 3.1	107.0 \pm 3.0
19	32.5 \pm 1.5	89.0 \pm 2.5	73.4 \pm 0.3	103.0 \pm 1.0
21	N.D. ^c	92.4 \pm 0.1	60.6 \pm 8.2	108.0 \pm 1.0

^aThe result is the average of duplicates with standard error shown.

^bThe result is the average of triplicates with standard derivation shown. ^cN.D. means "not determined". ^dThe experiments were conducted according to the Graves et al. procedure.⁵⁰

demonstrated a moderate level of plasma protein binding ranging from 85 to 96%. This level of plasma protein binding is unlikely to alter their bioavailability. Given the inhibitors had *K*_s approaching the subnanomolar range, the plasma proteins could be considered as carrier proteins that facilitate the their distribution.

Previously, sEH inhibitors with similar structures failed to show significant inhibition of the CYP450s which are highly involved in xenobiotic metabolism.⁴⁷ In this study, we examined the inhibition of CYP2C and CYP2J2 because CYP2C is an important drug metabolizing enzyme but principally because both enzymes are implicated in the synthesis of epoxy fatty acids.^{48–50} The results indicated that only minor inhibition of both CYP450 enzymes is observed at 10 μ M of the sEH inhibitors (Table 7). These data suggested that the sEH inhibitors do not affect the biosynthesis of EpFAs by inhibition of CYP2C and CYP2J2. This in turn suggests that the *in vivo* efficacy of the inhibitors is not due to inhibition upstream in the CYP450 pathway.

Inhibition of the hERG channel is a very important toxicology screen due to demonstrated association with cardiotoxicity. Most of the tested inhibitors show very minor inhibition on hERG at 50 μ M except for inhibitors **5** and **19** (Table 7). However, even inhibitors **5** and **19**, which have 0.49 and 0.31 nM *K*_i against recombinant human sEH, have more than an 10000-fold selectivity over the hERG channel. Therefore, these selected inhibitors are considered not to present a risk with hERG inhibition.

In summary, we have demonstrated that our sEH inhibitors having K_i value in the lower subnanomolar are unlikely to induce unanticipated side effects due to nonspecific binding to other pharmacologically important proteins. However, this does not completely rule out idiopathic off-target effects.

sEH Inhibitors Are Effective against an Animal Model of Type 1 Diabetic Neuropathic Pain. Several new potent sEH inhibitors with good pharmacokinetic profiles and no significant nonspecific binding on human proteins and enzymes were selected for further in vitro testing prior to in vivo studies. Because the in vivo studies were to be conducted in rat, we determined the potency (K_i and k_{off}) against the recombinant rat sEH (Table 8). The data suggest that the inhibitors have a

Table 8. In Vitro Potency of Selected sEH Inhibitors against Rat sEH

inhibitor	IC ₅₀ (nM) ^{a,b}	k_{off} ($\times 10^{-4}$ s ⁻¹) ^{a,c}	$t_{1/2}$ (min) ^{a,d}
18 (TPPU)	29.1 \pm 4.5	8.52 \pm 0.47	13.6 \pm 0.8
TPAU	79 \pm 2.5	9.70 \pm 0.14	11.9 \pm 0.18
4	1.8 \pm 0.1	3.26 \pm 0.72	36.6 \pm 8.2
7	<1.25	5.37 \pm 0.45	21.6 \pm 1.8
19	13.3 \pm 1.5	6.87 \pm 0.11	16.8 \pm 0.3
21	20 \pm 0.1	4.89 \pm 0.28	23.7 \pm 1.4

^aThe result is the average of triplicates with standard deviation (SD) shown. ^bIC₅₀ is determined by radiometric assay using [³H]-t-DPPO (50 μ M) as a substrate and rat sEH (2.5 nM) incubated at 30 °C for 10 min. ^c k_{off} was determined by FRET-based displacement assay described by Lee et al.³⁸ Briefly, a preincubated rat sEH–inhibitor complex (8 μ M) was diluted by $\times 40$ times by fluorescent reporter–APCU (2 μ M, 0.1 M sodium phosphate, pH 7.4). The fluorescent enhancement (λ_{excit} = 280 nm, λ_{emit} = 450) was measured over time (5100 s). The results are the average of triplicates with \pm SD. ^d $t_{1/2}$ = $\ln(2)/k_{\text{off}}$ which describes the half-life of enzyme–inhibitor complex.

slightly different structure–activity relationship (SAR) on the recombinant rat sEH compared to human sEH. The inhibitors with a 4-trifluoromethoxyphenyl– group at R₁ are less potent than the inhibitors with a 4-trifluoromethylphenyl– group at R₁ by at least 10-fold (Table 8). These results are opposite to the SAR obtained from the human recombinant sEH (Table 1 and 3). In addition, there is not a clear SAR based on the k_{off} of the inhibitors (Table 8). However, the results indicate that the new inhibitors are more potent, both in IC₅₀ and k_{off} , than the previously published inhibitors 18 (TPPU) and TPAU (Figure 1C and Table 8). Additionally, the pharmacokinetic profiles in rat were obtained for this new set of inhibitors (Supporting Information, Figure S11). All of the selected inhibitors show good oral bioavailability (PK-AUC) except inhibitor 21, which demonstrated at least 2 \times lower blood concentration than the other inhibitors (Table 9). Elimination is an important parameter of overall pharmacokinetics, and it has been previously reported that inhibitors with short elimination PK- $T_{1/2}$ are not well suited to use for chronic treatment.^{51,52} Several of the new inhibitors demonstrate good pharmacokinetic profiles with moderate elimination PK- $T_{1/2}$ (≥ 5 h) in both mice and rats. Therefore, these inhibitors were selected for further in vivo efficacy test on rat.

Because inhibitor 7 has the best in vitro potency (IC₅₀ and k_{off}) against rat sEH with a good pharmacokinetic profile (Table 8 and 9), it was tested in a model of type 1 diabetic neuropathic pain. At as low as 0.1 mg/kg, inhibitor 7 effectively increases mechanical withdrawal thresholds (reduces pain) in neuropathic rats (Figure 4A). Importantly, this reduction in

Table 9. Pharmacokinetic Parameters of Selected sEH Inhibitors Followed by Oral Dosing on Rat^a

structure	PK-AUC ^a (nM·h) ^b	C _{max} (nM) ^b	$T_{1/2}$ ^b (h)	T_{max} (h) ^b
4	7304	510	5.4	4
7	5716	790	4.9	1
19	12000	890	3.5	1
21	2590	297	4.2	4

^aThe rat ($n = 3$ or 4) were treated by oral dosing with a cassette of four compounds (0.3 mg/kg per each compound dissolved in 20% PEG400 in oleic acid rich triglycerides). ^bThe pharmacokinetic profiles of the inhibitors were calculated by Winonlin based on the best fit model of one compartmental analysis.

pain behavior increases dose dependently from 0.1 to 0.3 mg/kg (Figure 4A,B, $p < 0.05$). In addition, there is a good correlation between the blood concentration of inhibitor 7 and increased withdrawal thresholds (Figure 4C,D).

Our data indicate that inhibitor 7 shows better in vitro efficacy in terms of both IC₅₀ and k_{off} than the previously published inhibitor TPAU (Figure 1C) as well as having good pharmacokinetic profiles in both mouse and rat (Table 6 and 9). Therefore, we compared the in vivo efficacy of inhibitor 7 as previously reported results for TPAU in the same model. Our results indicate that using a 10-fold lower dose of inhibitor 7 is as efficacious as TPAU in the nociceptive bioassay (Figure 5).¹¹ It is also reassuring that the relative in vivo potency of these two sEH inhibitors in the nociceptive assays correlates with their relative in vitro potency on the target enzyme. These pain assays in the rat appear valuable for broad ranking of the analgesic activity of sEH inhibitors. However, the differences in pharmacokinetic and target site affinities caution against extrapolating these data to predict the fine ranking of the potency of different sEH inhibitors in man.

Overall, our data show that the new inhibitor 7 exhibits a strong correlation between in vivo efficacy with dose and drug level in blood, is more efficacious than the previously reported TPAU, and has promise as a therapy for use in treating chronic pain conditions.

CONCLUSION

Here, a new series of 1,3-disubstituted urea sEH inhibitors was synthesized with the design based on the recently obtained *holo*-structure of human sEH with inhibitor 18 (TPPU). The SAR of this new series indicates that the right side binding pocket of the sEH enzyme has limited space for optimization and is fluorophilic (Figures 1A, 2A,B), with an additional binding site identified in the left side binding pocket (Figures 1A, 2D). The newly synthesized inhibitors are at least 10 times more potent against human sEH than a previously published inhibitor (TPAU, Figure 1C, $K_{i(\text{human sEH})} = 9.4 \pm 0.3$ nM) with a minimum 2-fold longer residence time on the human sEH. These new inhibitors have been demonstrated selective for sEH with no significant specific binding toward several other human proteins (plasma protein, CYP450 enzymes, and hERG channel protein). The poor physical properties limit the oral bioavailability of inhibitors with a 1,3-disubstituted urea.^{18,30,31,34} This new series of inhibitors has improved physical properties translating into good pharmacokinetic profiles in the rat and mouse (Supporting Information, Figure S5–S11) increases their druglikeness compared to previous sEH inhibitors.

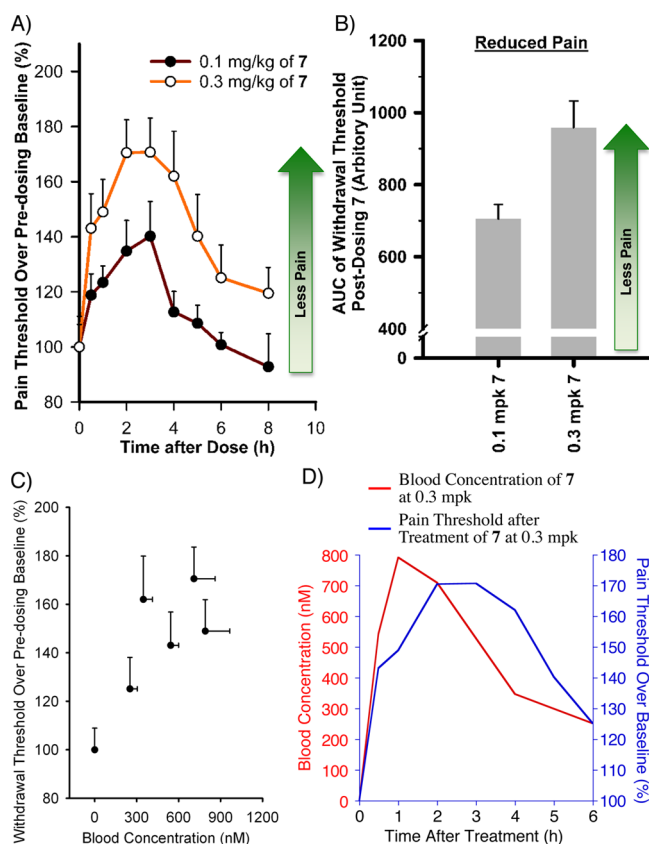


Figure 4. (A) Inhibitor 7 (IC_{50} rat sEH = <1.25 nM) improves mechanical withdrawal thresholds in a model of diabetic neuropathy. Oral dosing of 0.1 and 0.3 mg/kg dose dependently increased MWT, indicating pain relief ($n = 5$, mean \pm SEM). The neuropathic baseline is normalized to 100% to show the response to a single dose of sEH inhibitor over the time course. The response to treatments depended on the time, but when the treatments were compared, there was a statistically significant increase from the 0.1 to the 0.3 mg/kg dose (Mann–Whitney rank sum test, $U = 454.5$, $n_1 = n_2 = 45$, $p = <0.001$). (B) Inhibitor 7 shows dose dependent pain relief in diabetic rats. AUC describes an area under the curve of the MWT post-oral dosing of the inhibitor vs time. The bar chart depicts the AUC of MWTs after oral dosing of inhibitor 7. An increased in AUC of MWT is interpreted as an increase in pain relief. When the AUC for these doses were compared, this relationship maintained statistical significance (Mann–Whitney rank sum test, $U = 2.00$, $n_1 = n_2 = 5$, $p = 0.032$). (C) Efficacy in nociceptive assays relates to blood concentration. A plot of the nociceptive responses ($n = 5$, mean \pm SEM) vs blood concentration ($n = 4$, mean \pm SEM) reveals increasing efficacy with increasing blood concentration. (D) The efficacy of inhibitor 7 is dependent on blood concentration. When compared, the nociceptive responses ($n = 5$, mean \pm SEM) and the pharmacokinetic profile after oral dosing ($n = 4$, mean \pm SEM) of 7 follow the same trend while revealing a slight delay to in the behavioral assay. The graphics and statistics were prepared by KaleidaGraph version 4.1 (Synergy Software, Reading, PA).

Inhibiting sEH has been demonstrated to be more efficacious than gabapentin and celecoxib in alleviating modeled diabetic neuropathic pain in rat with no apparent side effect such as impaired mobility, cognition, or motor skill.^{10,11} However, the sEH inhibitors reported in those studies had either poor physical properties (poor water solubility and high melting point) or poor in vivo stability. In this report, the new more potent sEH inhibitors are close to 10 times more efficacious than TPAU in a diabetic neuropathic pain model. In addition,

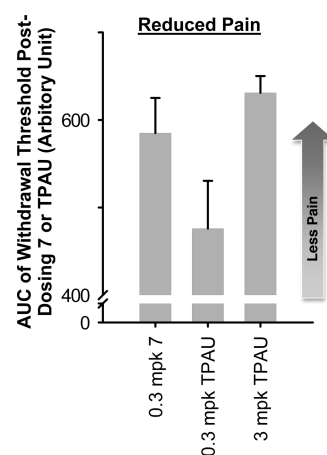


Figure 5. Newly optimized inhibitor 7 shows better in vivo efficacy in disease model. AUC describes an area under the curve of the withdrawal threshold post-oral dosing of the diabetic rat with sEH inhibitors vs time. A comparison of the newly synthesized sEH inhibitor 7 (IC_{50} rat sEH = <1.25 nM, $t_{1/2} = 21.6$ min) to previously published analogue TPAU (IC_{50} rat sEH = 79 nM, $t_{1/2} = 11.9$ min) showed a significantly higher response of inhibitor 7 at 0.3 mg/kg compared to the same 0.3 mg/kg dose of TPAU in a model of diabetic neuropathy (t test, $t = 2.31$ with 9 degrees of freedom, $p = 0.046$, * shows significant difference to 0.3 mpk of inhibitor 7). However, there was no significant difference between the 10-fold lower dose of inhibitor 7 at 0.3 mg/kg and TPAU at 3 mg/kg (Mann–Whitney rank sum test, $U = 14.00$, $n_1 = 5$, $n_2 = 6$, ns $p = 0.931$). The graphic and statistics were prepared by SigmaPlot (SysTat Software, San Jose, CA).

the selected inhibitor 7 demonstrated strong correlation between drug level in blood and dose with in vivo efficacy. This new series of inhibitors has demonstrated enhanced potency with slow k_{off} , improved pharmacokinetic profiles (moderate to long elimination $T_{1/2}$ and high AUC), and more importantly, improved efficacy against diabetic neuropathic pain in a rat model. With increased potency and bioavailability, there are decreases in the required effective dose and greatly simplified formulation. The new sEH inhibitors are good candidates for chronic treatment of diabetic neuropathic pain.

EXPERIMENTAL SECTION

General. All reagents and solvent were purchased from commercial suppliers and were used directly without further purifications. All syntheses were carried out in a dry nitrogen atmosphere unless otherwise specified. Reactions were monitored by thin-layer chromatography (TLC) on Merck F_{254} silica gel 60 aluminum sheets, and spots were either visible under light or UV light (254 nm) or stained with an oxidizing solution ($KMnO_4$ stain). The same TLC system was used to test purity, and all final products showed a single spot on TLC. Column chromatography was performed with silica gel.

1H NMR spectra were recorded on a Varian QE-300 spectrometer with deuterated chloroform ($CDCl_3$; $\delta = 7.24$ ppm) or deuterated dimethyl sulfoxide ($DMSO-d_6$) containing TMS as an internal standard. ^{13}C NMR spectra were recorded on a Varian QE-300 spectrometer at 75 MHz.

The purity of the inhibitors reported in this manuscript was determined either by (1) HPLC-UV using Agilent 1200 series HPLC series equipped with Phenomenex Luna2 C18 reverse phase column (C18, 4.6 mm \times 150 mm, 5 μm) coupled with Agilent G1314 UV–vis detector (detection at 230 nm) with isocratic flow at methanol:water (2:1 by volume) for 90 min, or by (2) 1H NMR. The lowest obtained purity was reported. The inhibitor was dissolved in EtOH at 100 μM and 10 μL was injected on HPLC. Purity was based on the percent of total peak area at 230 nm using HPLC-UV. This purity estimate was

compared with that from the ¹H NMR. The presence of anilines in the final product was estimated from ¹H NMR. The lowest obtained purity was reported. The purity was also further supported as described in the Supporting Information by LC/MS with monitoring of total ion current, TLC in several systems, a sharp melting point, and occasional other technique. The elemental analysis was conducted by MIDWESTMICRO lab, LCC.

The synthesis of *tert*-butyl 4-(3-(4-(trifluoromethyl)phenyl)ureido)-piperidine-1-carboxylate, 1-(piperidin-4-yl)-3-(4-(trifluoromethyl)phenyl)urea, 1-(piperidin-4-yl)-3-(4-(trifluoromethoxy)phenyl)urea and *tert*-butyl 4-(3-(4-(trifluoromethoxy)phenyl)ureido)piperidine-1-carboxylate have been reported elsewhere.^{23,30,53} The synthesis of inhibitors **1**,³⁸ **2**,²³ **3**,²³ **6**,³⁸ APAU,³² TPAU,²³ **18** (TPPU),²³ **20** (TPCU),²³ and t-TUCB³⁴ were reported elsewhere. Experimental of each individual inhibitor is described in Supporting Information in detail.

The experimental procedures of enzyme preparation, IC₅₀ determination for sEH inhibitors, and K_i determination for sEH inhibitors followed the published procedures and are described in detail in Supporting Information.^{38,54–58}

Synthetic Method 1. Step 1. Corresponding isocyanate (1 equiv) and 4-amino-1-Boc-piperidine (1.1 equiv) were dissolved in CH₂Cl₂ (50 mM, corresponding to isocyanate) and stirred at rt for 12 h. The reaction was quenched by addition of water. The organic layer was isolated, and the aqueous layer was extracted with EtOAc (EtOAc:aqueous layer/1:1) four times. The combined organic layer was dried over anhydrous magnesium sulfate and was concentrated under vacuo and was further purified by flash chromatography, yielding corresponding Boc-protected urea.

Step 2. The BOC protected urea from the step 1 was dissolved in HCl solution (2M, MeOH) to make reaction mixture (186 mM, BOC protected urea). The resulting solution was refluxed for 2 h. The solvent was removed in vacuo, and the crude reaction product was adjusted to pH 12 with NaOH solution (6N). The precipitates were filtered and dried under high vacuum. The final product unprotected urea was served as a scaffold for the next step of synthesis.

Step 3. Unless specified, the unprotected urea (1 equiv) from step 2, EDCI (1.5 equiv), DMAP (1.5 equiv), and corresponding carboxylic acid (1.5 equiv) were dissolved in CH₂Cl₂ (8.3 mM, unprotected urea) and stirred overnight (12 h) at rt. The reaction was quenched by addition of HCl solution (1M). The organic layer was collected, and the aqueous layer was extracted with EtOAc (EtOAc:aqueous layer/1:1) four times. The combined organic layer was dried over anhydrous magnesium sulfate and was concentrated in vacuo and further purified by flash chromatography.

Synthetic Method 2. The corresponding isocyanate (1 equiv) was added to a suspension of targeted piperidine (1.1 equiv) in CH₂Cl₂ (20 mM, corresponding isocyanate). The reaction was stirred overnight (12 h) at rt. The reaction was quenched with the addition of HCl solution (2M). The organic layer was collected, and the aqueous layer was further extracted with EtOAc (EtOAc:aqueous layer/1:1) three times. The combined organic layer was washed with satd NaCl solution. The organic layer was dried over anhydrous magnesium sulfate and was concentrated in vacuo. The product was purified by flash chromatography.

Synthetic Method 3. Corresponding amine (1 equiv) and triethylamine (1.2 equiv) was dissolved in CH₂Cl₂ (54 mM corresponding to amine) and stirred at –78 °C. Triphosgene (0.37 equiv) dissolved in CH₂Cl₂ (20 mM, corresponding triphosgene) was added dropwise at –78 °C. The reaction was then warm to rt and was stirred for 30 min. The reaction was cooled to 0 °C. Corresponding piperidine (1.1 equiv) dissolved in CH₂Cl₂ (54 mM, corresponding piperidine) was added slowly, and the reaction was further stirred at rt for 12 h. The reaction was quenched with the addition of HCl solution (2M). The organic layer was collected, and the aqueous layer was further extracted with EtOAc (EtOAc:aqueous layer/1:1) three times. The combined organic layer was washed with satd NaCl solution. The organic layer was dried over anhydrous magnesium sulfate and was concentrated in vacuo. The product was purified by flash chromatography.

Synthetic Method 4. The first two steps are the same as synthetic method 1, steps 1 and 2, unless specified.

Step 3. The unprotected urea (1 equiv) and triethylamine (1.2 equiv) was dissolved in CH₂Cl₂ (8.3 mM, corresponding unprotected urea), and corresponding sulfonyl chloride was added dropwise at 0 °C and the reaction was stirred overnight (12 h) at rt. The reaction was quenched by addition of HCl solution (1M). The organic layer was collected, and the aqueous layer was extracted with EtOAc (EtOAc:aqueous layer/1:1) four times. The combined organic layer was dried over anhydrous magnesium sulfate and was concentrated in vacuo and further purified by flash chromatography.

Protein Crystallization. Crystals of the enzyme were obtained using the hanging drop vapor-diffusion method by mixing equal volumes of protein (8–12 mg/mL concentration in 100 mM sodium phosphate pH 7.4, 3 mM DTT) and the reservoir solution (30% PEG 3350, 0–10% sucrose) at 4 °C. The crystals grew in approximately 1 week and belonged to the hexagonal space group P6₃22.

Complexes of sEH with inhibitors **8**/UC1770 or **4** have been obtained by soaking sEH crystals grown as described above in modified mother liquor (35% PEG 3350, 50 mM sodium phosphate pH 7.4) supplemented with 1 mM solution of inhibitor for 1–7 days

Data Collection. Prior to the data collection, a suitable crystal was dipped for 30 s in a modified mother liquor solution (35% PEG 3350) with the addition of 10% glycerol as a cryoprotectant. Diffraction data were collected at 100 K at the XP station at the Center for Advance Microstructures and Devices at Louisiana State University with a MAR charge-coupled device camera (structure TPPU/UC1770) or the NE-CAT beamline 24-ID-C at the Advanced Photon Source equipped with the Pilatus 6 M detector (structure **4**). The images were processed and scaled using the HKL2000 (structure TPPU/UC1770)⁵⁹ or Xia2 program suit⁶⁰ (structure **4**). Data collection and data processing statistics are given in Table 1.

Crystal Structure Determination. The molecular replacement procedure was applied to locate a solution using the program MOLREP.⁶¹ A monomer of human sEH (PDB accession code 1S8O) was used as a search model. The positioned MR model was refined using the maximum likelihood refinement in REFMAC⁶¹ with the TLS parameters generated by the TLSMD server.⁶² Program Coot was used for model building throughout the refinement.⁶³

HERG Patch Clamp Measurement. Cell Culture for Channel Analysis. HEK-293 cells stably expressing hKv11.1 (hERG) under G418 selection were a generous gift from Craig January (University of Wisconsin, Madison). Cells were cultured in DMEM containing 10% fetal bovine serum, 2 mM glutamine, 1 mM Na⁺ pyruvate, 100 U/mL penicillin and 100 µg/mL streptomycin, and 500 mg/mL G418. Before electrophysiological experiments, cells were grown to 60% confluency and 10 mM astemizole was added to the culture for 24 h to increase Kv11.1 surface expression.

Electrophysiology. All experiments were conducted with an EPC-10 amplifier (HEKA, Lambrecht/Pfalz, Germany) in the whole-cell configuration of the patch-clamp technique with a holding potential of –80 mV. Pipette resistances averaged 2.0 MΩ. Compound solutions in Na⁺-Ringer were freshly prepared during the experiments from 10 mM stock solutions in DMSO. The final DMSO concentration never exceeded 1%. The external solution contained in mM: 160 NaCl, 4.5 KCl, 2 CaCl₂, 1 MgCl₂, and 10 HEPES, pH 7.4, osmolality 300 mmol/kg. The internal pipet solution contained in mM: 120 KCl, 10 HEPES, 4 Na₂ATP, 10 EGTA, 5.374 CaCl₂, 1.75 MgCl₂, pH 7.2, osmolality 295 mmol/kg (free Ca²⁺ concentration 150 nM calculated with MaxChelator assuming a temperature of 25 °C, a pH of 7.2, and an ionic strength of 160 mM). HERG (Kv11.1) currents were elicited with a two-step pulse (applied every 10 s) from –80 mV first to 20 mV for 1 s and then to –50 mV for 2 s, and the percent reduction of both peak and tail current by the drug were determined.

Pharmacokinetic Study of Inhibitors Using Oral Dosing in Mice. All the animal experiments were performed according to the protocols approved by the Animal Use and Care Committee of University of California—Davis. Male Swiss Webster mice (8 week old, 24–30 g) purchased from Charles River Laboratories were used for PK studies. Inhibitors for oral administration were dissolved in

oleic acid-rich triglyceride containing 20% PEG400 (v/v) to give a clear solution. Blood (10 μ L) was collected from the tail vein using a pipet tip rinsed with 7.5% EDTA(K_3) at 0, 0.5, 1, 1.5, 2, 4, 6, 8, 24, and 48 h after administration of the inhibitor in a cassette of 3–5 compounds (Supporting Information, Table S1) (0.3 mg/kg per compounds, 100–110 μ L). Each group contained 3–4 animals. Each blood sample was immediately transferred to a tube containing 50 μ L of water containing 0.1% EDTA. After being mixed strongly on a Vortex for 1 min, all samples were stored at -80°C until analysis. The blood samples were prepared for the measurement of sEH inhibitors according to the previously reported method by Liu et al.¹⁸ The details LC/MS–MS methods are described in detail in the Supporting Information.

Pharmacokinetic Study of Inhibitors Using Oral Dosing in Rat. All the animal experiments were performed according to the protocols approved by the Animal Use and Care Committee of University of California—Davis. Male Sprague–Dawley rats ($n = 4$, 8 week old, 250–300 g) were used for pharmacokinetic study for sEH inhibitors. A cassette of four inhibitors (inhibitors 4, 7, 19, and 21, 0.3 mg/kg per inhibitors, 0.9–1.2 mL) was given by oral administration. Inhibitor was dissolved in oleic oil containing 5% polyethylene glycol 400 to form a clear solution. Blood (10 μ L) was collected from the tail vein by using a pipet tip rinsed with 7.5% EDTA(K_3) at 0, 0.5, 1, 1.5, 2, 4, 6, 8, and 24 h after oral dosing with the inhibitor. Each blood sample was immediately transferred to a tube containing 50 μ L of water and mixed by vortex for 1 min, and all samples were stored at -80°C until analysis. The blood samples were prepared for the measurement of sEH inhibitors according to the previously reported method by Liu et al.¹⁸ The details LC/MS–MS methods are described in detail in the Supporting Information.

Diabetic Neuropathic Pain Model. A diabetic neuropathic pain modeled was generated using streptozocin which targets and kills the pancreatic beta islet cells, rendering the animals with type I diabetes. The rats were acclimated for 1 h and tested for baseline thresholds before inducing diabetes. The baseline mechanical withdrawal thresholds were established using the von Frey mechanical nociceptive test with an electronic anesthesiometer (IITC, Woodland Hills, CA). Subsequently, streptozocin (55 mg/kg) in saline was injected via tail vein per previously reported methods.⁶⁴ After 5 days, the allodynia of diabetic rats was confirmed with the von Frey nociceptive assay. Rats were placed in clear acrylic chambers on a steel mesh floor. The hind paw of the rat was probed through the mesh with a rigid tip probe connected to the electronic readout pressure meter set to the maximum hold setting. The withdrawal thresholds per rat were measured 3–5 times at 1 min intervals for each time point.

The baseline diabetic allodynia was quantified again at the beginning of all test days. The rats were then administered vehicle or sEH inhibitor via oral gavage and tested at 30 min, 1, 2, 3, 4, 5, 6, and 8 h for mechanical withdrawal thresholds. The reported scores are the grams of force required to elicit a hind paw withdrawal averaged with standard error of the mean (SEM) per a group of rats ($n = 5$). The baseline diabetic neuropathic scores were normalized to 100% to reflect the response to treatments which are reported as % of post diabetic neuropathic baseline.

■ ASSOCIATED CONTENT

● Supporting Information

Correlation plot between k_{off} against number of non-hydrogen atom, experimental log P and K_i ; plots of pharmacokinetic profiles of selected inhibitors in mice and rat; detailed experimental on chemistry, biochemistry, and animal studies; tables of optimized conditions for monitoring sEH inhibitors by MRM. This material is available free of charge via the Internet at <http://pubs.acs.org>.

Accession Codes

PDB accession codes: 4OD0 (human sEH with inhibitor 18 (UC1770/TPPU)) and 4OCZ (human sEH with inhibitor 4 (UC2389)).

■ AUTHOR INFORMATION

Corresponding Author

*Phone: 530-752-7519. Fax: 530-752-1537. E-mail: bdhammock@ucdavis.edu.

Notes

The authors declare the following competing financial interest(s): The University of California holds patents on the sEH inhibitors used in this study as well as their use to treat inflammation, inflammatory pain, and neuropathic pain. B.D. Hammock is a co-founder of Eicosis L.L.C., a start up company advancing sEH inhibitors into the clinic. All the others co-authors declare no competing financial interest.

■ ACKNOWLEDGMENTS

This work was partially funded by NIEHS grant R01 ES002710, NIAMS grant R21 AR062866, NIH CounterAct US4 NS079202, and NIEHS Superfund Research Program grant P42 ES004699. B.D.H. is a George and Judy Marcus Senior Fellow of the American Asthma Foundation. This work was supported in part by NIH R01 HL107887 (M.E.N.) and by the Louisiana Governors' Biotechnology Initiative. Data for the structure TPPU (UC1770) were collected at the Gulf Coast Protein Crystallography Beamline at the Center for Advanced Microstructures and Devices. This beamline is supported by the National Science Foundation grant DBI-9871464 with cofunding from the National Institute of General Medical Sciences. Data for the structure of inhibitor 4 (UC2389) were collected at the Advanced Photon Source on the Northeastern Collaborative Access Team beamlines, which are supported by grants from the National Center for Research Resources (P41RR015301-10) and the National Institute of General Medical Sciences (P41 GM103403-10) from the National Institutes of Health. Use of the Advanced Photon Source, an Office of Science User Facility operated for the U.S. Department of Energy (DOE) Office of Science by Argonne National Laboratory, was supported by the U.S. DOE under contract no. DE-AC02-06CH11357. We thank Dr. Henry Bellami and Dr. David Neau for assistance with data collection.

■ ABBREVIATIONS USED

sEH, soluble epoxide hydrolase; EpFAs, epoxy fatty acids; CYP450, cytochrome P450; EETs, epoxy-eicosatrienoic acids; EpETEs, epoxy-eicosatetraenoic acids; EpDPEs, epoxy-docosapentaenoic acids; K_i , inhibition constant; K_d , dissociation constant; TPPU, 1-trifluoromethoxyphenyl-3-(1-propionylpiperidin-4-yl) urea; k_{off} , dissociation rate constant; eLogP, experimental Log P ; PK-AUC, area under the curve of the pharmacokinetic profiles; TUPS, 1-(1-methylsulfonyl-piperidin-4-yl)-3-(4-trifluoromethoxyphenyl)-urea; TPAU, 1-trifluoromethoxyphenyl-3-(1-acetylpiperidin-4-yl)-urea; APAU, 1-(1-acetylpiperidin-4-yl)-3-adamantanyleurea; KMnO_4 , potassium permanganate; *t*-TUCB, *trans*-4-[4-[3-(4-trifluoromethoxyphenyl)-uredio]-cyclohexyloxy]benzoic acid; EDCI, 1-ethyl-3-(3-(dimethylamino)propyl)carbodiimide; EtOAc, ethyl acetate; MeOH, methanol; HCl, hydrochloric acid; NaOH, sodium hydroxide; DMAP, 4-dimethylaminopiperidine; MRM, multiple reaction monitoring; MWT, mechanical withdrawal thresholds

■ REFERENCES

(1) *National Diabetes Fact Sheet: National Estimates and General Information on Diabetes and Prediabetes in the United States*; U.S.

Department of Health and Human Services, Centers for Disease Control and Prevention: Atlanta, GA, 2011.

(2) Calcutt, N. A. Tolerating diabetes: an alternative therapeutic approach for diabetic neuropathy. *ASN Neuro* **2010**, *2*, 216–217.

(3) Said, G. Diabetic neuropathy—a review. *Nature Clin. Pract. Neurol.* **2007**, *3*, 331–340.

(4) Veves, A.; Backonja, M.; Malik, R. A. Painful diabetic neuropathy: epidemiology, natural history, early diagnosis, and treatment options. *Pain Med.* **2008**, *9*, 660–674.

(5) Wong, M.-c.; Chung, J. W. Y.; Wong, T. K. S. Effects of treatments for symptoms of painful diabetic neuropathy: systematic review. *BMJ n(Br. Med. J.)* **2007**, *335*, 87.

(6) Spector, A. A. Arachidonic acid cytochrome P450 epoxygenase pathway. *J. Lipid Res.* **2009**, *50*, S52–S56.

(7) Morisseau, C.; Inceoglu, B.; Schmelzer, K.; Tsai, H.-J.; Jinks, S. L.; Hegedus, C. M.; Hammock, B. D. Naturally occurring monoepoxides of eicosapentaenoic acid and docosahexaenoic acid are bioactive antihyperalgesic lipids. *J. Lipid Res.* **2010**, *51*, 3481–3490.

(8) Wagner, K.; Inceoglu, B.; Gill, S. S.; Hammock, B. D. Epoxygenated Fatty Acids and Soluble Epoxide Hydrolase Inhibition: Novel Mediators of Pain Reduction. *J. Agric. Food Chem.* **2011**, *59*, 2816–2824.

(9) Morisseau, C.; Hammock, B. D. Impact of Soluble Epoxide Hydrolase and Epoxyeicosanoids on Human Health. *Annu. Rev. Pharmacol. Toxicol.* **2013**, *53*, 37–58.

(10) Wagner, K.; Inceoglu, B.; Dong, H.; Yang, J.; Hwang, S. H.; Jones, P.; Morisseau, C.; Hammock, B. D. Comparative efficacy of 3 soluble epoxide hydrolase inhibitors in rat neuropathic and inflammatory pain models. *Eur. J. Pharmacol.* **2013**, *700*, 93–101.

(11) Inceoglu, B.; Wagner, K. M.; Yang, J.; Bettaieb, A.; Schebb, N. H.; Hwang, S. H.; Morisseau, C.; Haj, F. G.; Hammock, B. D. Acute augmentation of epoxyeicosanoid levels rapidly reduces pain-related behavior in a rat model of type I diabetes. *Proc. Natl. Acad. Sci. U. S. A.* **2012**, *109*, 11390–11395.

(12) Guedes, A. G. P.; Morisseau, C.; Sole, A.; Soares, J. H. N.; Ulu, A.; Dong, H.; Hammock, B. D. Use of a soluble epoxide hydrolase inhibitor as an adjunctive analgesic in a horse with laminitis. *Vet. Anaesth. Analg.* **2013**, *40*, 440–448.

(13) Tran, L.; Kompa, A. R.; Wang, B. H.; Krum, H. Evaluation of the Effects of Urotensin II and Soluble Epoxide Hydrolase Inhibitor on Skin Microvessel Tone in Healthy Controls and Heart Failure Patients. *Cardiovasc. Ther.* **2012**, *30*, 295–300.

(14) Ai, D.; Pang, W.; Li, N.; Xu, M.; Jones, P. D.; Yang, J.; Zhang, Y.; Chiamvimonvat, N.; Shyy, J. Y. J.; Hammock, B. D.; Zhu, Y. Soluble epoxide hydrolase plays an essential role in angiotensin II-induced cardiac hypertrophy. *Proc. Natl. Acad. Sci. U. S. A.* **2009**, *106*, 564–569.

(15) Brenneis, C.; Sisignano, M.; Coste, O.; Altenrath, K.; Fischer, M. J.; Angioni, C.; Fleming, I.; Brandes, R. P.; Reeh, P. W.; Woolf, C. J.; Geisslinger, G.; Scholich, K. Soluble epoxide hydrolase limits mechanical hyperalgesia during inflammation. *Mol. Pain* **2011**, *7*, 78.

(16) Imig, J. D.; Hammock, B. D. Soluble epoxide hydrolase as a therapeutic target for cardiovascular diseases. *Nature Rev. Drug Discovery* **2009**, *8*, 794–805.

(17) Inceoglu, B.; Jinks, S. L.; Schmelzer, K. R.; Waite, T.; Kim, I. H.; Hammock, B. D. Inhibition of soluble epoxide hydrolase reduces LPS-induced thermal hyperalgesia and mechanical allodynia in a rat model of inflammatory pain. *Life Sci.* **2006**, *79*, 2311–2319.

(18) Liu, J.-Y.; Lin, Y.-P.; Qiu, H.; Morisseau, C.; Rose, T. E.; Hwang, S. H.; Chiamvimonvat, N.; Hammock, B. D. Substituted phenyl groups improve the pharmacokinetic profile and anti-inflammatory effect of urea-based soluble epoxide hydrolase inhibitors in murine models. *Eur. J. Pharm. Sci.* **2013**, *48*, 619–627.

(19) Schmelzer, K. R.; Kubala, L.; Newman, J. W.; Kim, I. H.; Eiserich, J. P.; Hammock, B. D. Soluble epoxide hydrolase is a therapeutic target for acute inflammation. *Proc. Natl. Acad. Sci. U. S. A.* **2005**, *102*, 9772–9777.

(20) Ulu, A.; Harris, T. R.; Morisseau, C.; Miyabe, C.; Inoue, H.; Schuster, G.; Dong, H.; Iosif, A.-M.; Liu, J.-Y.; Weiss, R. H.;

Chiamvimonvat, N.; Imig, J. D.; Hammock, B. D. Anti-inflammatory Effects of omega-3 Polyunsaturated Fatty Acids and Soluble Epoxide Hydrolase Inhibitors in Angiotensin-II-Dependent Hypertension. *J. Cardiovasc. Pharmacol.* **2013**, *62*, 285–297.

(21) Shen, H. C.; Hammock, B. D. Discovery of Inhibitors of Soluble Epoxide Hydrolase: A Target with Multiple Potential Therapeutic Indications. *J. Med. Chem.* **2012**, *55*, 1789–1808.

(22) Shen, H. C.; Ding, F.-X.; Wang, S.; Deng, Q.; Zhang, X.; Chen, Y.; Zhou, G.; Xu, S.; Chen, H.-S.; Tong, X.; Tong, V.; Mitra, K.; Kumar, S.; Tsai, C.; Stevenson, A. S.; Pai, L.-Y.; Alonso-Galicia, M.; Chen, X.; Soisson, S. M.; Roy, S.; Zhang, B.; Tata, J. R.; Berger, J. P.; Colletti, S. L. Discovery of a Highly Potent, Selective, and Bioavailable Soluble Epoxide Hydrolase Inhibitor with Excellent ex Vivo Target Engagement. *J. Med. Chem.* **2009**, *52*, S009–S012.

(23) Rose, T. E.; Morisseau, C.; Liu, J.-Y.; Inceoglu, B.; Jones, P. D.; Sanborn, J. R.; Hammock, B. D. 1-Aryl-3-(1-acylpiperidin-4-yl)urea Inhibitors of Human and Murine Soluble Epoxide Hydrolase: Structure–Activity Relationships, Pharmacokinetics, and Reduction of Inflammatory Pain. *J. Med. Chem.* **2010**, *53*, 7067–7075.

(24) Reema, K. T.; McAtee, J. J.; Belyanskaya, S.; Brandt, M.; Brown, G. D.; Costell, M. H.; Ding, Y.; Dodson, J. W.; Eisennagel, S. H.; Fries, R. E.; Gross, J. W.; Harpel, M. R.; Holt, D. A.; Israel, D. I.; Jolivet, L. J.; Krosky, D.; Li, H.; Lu, Q.; Mandichak, T.; Roethke, T.; Schnackenberg, C. G.; Schwartz, B.; Shewchuk, L. M.; Xie, W.; Behm, D. J.; Douglas, S. A.; Shaw, A. L.; Marino, J. P., Jr. Discovery of 1-(1,3,5-triazin-2-yl)piperidine-4-carboxamides as inhibitors of soluble epoxide hydrolase. *Bioorg. Med. Chem. Lett.* **2013**, *23*, 3584–3588.

(25) Podolin, P. L.; Bolognese, B. J.; Foley, J. F.; Long, E., III; Peck, B.; Umbrecht, S.; Zhang, X.; Zhu, P.; Schwartz, B.; Xie, W.; Quinn, C.; Qi, H.; Sweitzer, S.; Chen, S.; Galop, M.; Ding, Y.; Belyanskaya, S. L.; Israel, D. I.; Morgan, B. A.; Behm, D. J.; Marino, J. P., Jr.; Kurali, E.; Barnette, M. S.; Mayer, R. J.; Booth-Genthe, C. L.; Callahan, J. F. In vitro and in vivo characterization of a novel soluble epoxide hydrolase inhibitor. *Prostaglandins Other Lipid Mediators* **2013**, *104*, 25–31.

(26) Kim, I.-H.; Nishi, K.; Tsai, H.-J.; Bradford, T.; Koda, Y.; Watanabe, T.; Morisseau, C.; Blanchfield, J.; Toth, I.; Hammock, B. D. Design of bioavailable derivatives of 12-(3-adamantan-1-yl-ureido)-dodecanoic acid, a potent inhibitor of the soluble epoxide hydrolase. *Bioorg. Med. Chem. Lett.* **2007**, *15*, 312–323.

(27) Huang, S.-X.; Cao, B.; Morisseau, C.; Tin, Y.; Hammock, B. D.; Long, Y.-Q. Structure-based optimization of the piperazino-containing 1,3-disubstituted ureas affording sub-nanomolar inhibitors of soluble epoxide hydrolase. *MedChemComm* **2012**, *3*, 379–384.

(28) Morisseau, C.; Goodrow, M. H.; Dowdy, D.; Zheng, J.; Greene, J. F.; Sanborn, J. R.; Hammock, B. D. Potent urea and carbamate inhibitors of soluble epoxide hydrolases. *Proc. Natl. Acad. Sci. U. S. A.* **1999**, *96*, 8849–8854.

(29) Kim, I.-H.; Tsai, H.-J.; Nishi, K.; Kasagami, T.; Morisseau, C.; Hammock, B. D. 1,3-Disubstituted ureas functionalized with ether groups are potent inhibitors of the soluble epoxide hydrolase with improved pharmacokinetic properties. *J. Med. Chem.* **2007**, *50*, S217–S226.

(30) Hwang, S. H.; Tsai, H.-J.; Liu, J.-Y.; Morisseau, C.; Hammock, B. D. Orally bioavailable potent soluble epoxide hydrolase inhibitors. *J. Med. Chem.* **2007**, *50*, 3825–3840.

(31) Liu, J. Y.; Tsai, H. J.; Hwang, S. H.; Jones, P. D.; Morisseau, C.; Hammock, B. D. Pharmacokinetic optimization of four soluble epoxide hydrolase inhibitors for use in a murine model of inflammation. *Br. J. Pharmacol.* **2009**, *156*, 284–296.

(32) Jones, P. D.; Tsai, H. J.; Do, Z. N.; Morisseau, C.; Hammock, B. D. Synthesis and SAR of conformationally restricted inhibitors of soluble epoxide hydrolase. *Bioorg. Med. Chem. Lett.* **2006**, *16*, S212–S216.

(33) Copeland, R. A.; Pompliano, D. L.; Meek, T. D. Opinion—Drug–target residence time and its implications for lead optimization. *Nature Rev. Drug Discovery* **2006**, *5*, 730–739.

(34) Tsai, H.-J.; Hwang, S. H.; Morisseau, C.; Yang, J.; Jones, P. D.; Kasagami, T.; Kim, I.-H.; Hammock, B. D. Pharmacokinetic screening

of soluble epoxide hydrolase inhibitors in dogs. *Eur. J. Pharm. Sci.* **2010**, *40*, 222–238.

(35) Lewis, D. F. V.; Jacobs, M. N.; Dickins, M. Compound lipophilicity for substrate binding to human P450s in drug metabolism. *Drug Discovery Today* **2004**, *9*, 530–537.

(36) Hagmann, W. K. The many roles for fluorine in medicinal chemistry. *J. Med. Chem.* **2008**, *51*, 4359–4369.

(37) Jeschke, P. *The Unique Role of Halogen Substituents in the Design of Modern Crop Protection Compounds*; Wiley-VCH Verlag GmbH & Co. KGaA: Weinheim, Germany, 2012.

(38) Lee, K. S. S.; Morisseau, C.; Yang, J.; Wang, P.; Hwang, S. H.; Hammock, B. D. Forster resonance energy transfer competitive displacement assay for human soluble epoxide hydrolase. *Anal. Biochem.* **2013**, *434*, 259–268.

(39) Gomez, G. A.; Morisseau, C.; Hammock, B. D.; Christianson, D. W. Human soluble epoxide hydrolase: structural basis of inhibition by 4-(3-cyclohexylureido)-carboxylic acids. *Protein Sci.* **2006**, *15*, 58–64.

(40) Allen, F. H.; Kennard, O.; Watson, D. G.; Brammer, L.; Orpen, A. G.; Taylor, R. Tables of bond lengths determined by x-ray and neutron diffraction. Part 1. Bond lengths in organic compounds. *J. Chem. Soc., Perkin Trans.* **1987**, *2*, S1–S19.

(41) Ulu, A.; Appt, S. E.; Morisseau, C.; Hwang, S. H.; Jones, P. D.; Rose, T. E.; Dong, H.; Lango, J.; Yang, J.; Tsai, H. J.; Miyabe, C.; Fortenbach, C.; Adams, M. R.; Hammock, B. D. Pharmacokinetics and in vivo potency of soluble epoxide hydrolase inhibitors in cynomolgus monkeys. *Br. J. Pharmacol.* **2012**, *165*, 1401–1412.

(42) Vickers, A. E. M.; Sinclair, J. R.; Zollinger, M.; Heitz, F.; Glanzel, U.; Johanson, L.; Fischer, V. Multiple cytochrome P-450s involved in the metabolism of terbinafine suggest a limited potential for drug–drug interactions. *Drug Metab. Dispos.* **1999**, *27*, 1029–1038.

(43) Austin, R. P.; Barton, P.; Cockcroft, S. L.; Wenlock, M. C.; Riley, R. J. The influence of nonspecific microsomal binding on apparent intrinsic clearance, and its prediction from physicochemical properties. *Drug Metab. Dispos.* **2002**, *30*, 1497–1503.

(44) O'Brien, A. J.; Fullerton, J. N.; Massey, K. A.; Auld, G.; Sewell, G.; James, S.; Newson, J.; Karra, E.; Winstanley, A.; Alazawi, W.; Garcia-Martinez, R.; Cordoba, J.; Nicolaou, A.; Gilroy, D. W. Immunosuppression in acutely decompensated cirrhosis is mediated by prostaglandin E-2. *Nature Med.* **2014**, *20*, 522–527.

(45) Wu, J.; LoRusso, P. M.; Matherly, L. H.; Li, J. Implications of Plasma Protein Binding for Pharmacokinetics and Pharmacodynamics of the gamma-Secretase Inhibitor RO492097. *Clin. Cancer. Res.* **2012**, *18*, 2066–2079.

(46) Smith, D. A.; Di, L.; Kerns, E. H. The effect of plasma protein binding on in vivo efficacy: misconceptions in drug discovery. *Nature Rev. Drug Discovery* **2010**, *9*, 929–939.

(47) Morisseau, C.; Merzlikin, O.; Lin, A.; He, G.; Feng, W.; Padilla, I.; Denison, M. S.; Pessah, I. N.; Hammock, B. D. Toxicology in the fast lane: application of high-throughput bioassays to detect modulation of key enzymes and receptors. *Environ. Health Perspect.* **2009**, *117*, 1867–1872.

(48) Zeldin, D. C.; Moomaw, C. R.; Jesse, N.; Tomer, K. B.; Beetham, J.; Hammock, B. D.; Wu, S. Biochemical characterization of the human liver cytochrome P450 arachidonic acid epoxigenase pathway. *Arch. Biochem. Biophys.* **1996**, *330*, 87–96.

(49) Wu, S.; Moomaw, C. R.; Tomer, K. B.; Falck, J. R.; Zeldin, D. C. Molecular cloning and expression of CYP2J2, a human cytochrome P450 arachidonic acid epoxigenase highly expressed in heart. *J. Biol. Chem.* **1996**, *271*, 3460–3468.

(50) Graves, J. P.; Edin, M. L.; Bradbury, J. A.; Gruzdev, A.; Cheng, J.; Lih, F. B.; Masinde, T. A.; Qu, W.; Clayton, N. P.; Morrison, J. P.; Tomer, K. B.; Zeldin, D. C. Characterization of four new mouse cytochrome P450 enzymes of the CYP2J subfamily. *Drug Metab. Dispos.* **2013**, *41*, 763–773.

(51) Chiang, P.-C.; Ran, Y.; Chou, K.-J.; Cui, Y.; Wong, H. Investigation of utilization of nanosuspension formulation to enhance exposure of 1,3-dicyclohexylurea in rats: preparation for PK/PD study via subcutaneous route of nanosuspension drug delivery. *Nanoscale Res. Lett.* **2011**, *6*, 413.

(52) Chiang, P.-C.; La, H.; Zhang, H.; Wong, H. Systemic Concentrations Can Limit the Oral Absorption of Poorly Soluble Drugs: An Investigation of Non-Sink Permeation Using Physiologically Based Pharmacokinetic Modeling. *Mol. Pharmacol.* **2013**, *10*, 3980–3988.

(53) Jones, P. D.; Tsai, H.-J.; Do, Z. N.; Morisseau, C.; Hammock, B. D. Synthesis and SAR of conformationally restricted inhibitors of soluble epoxide hydrolase. *Bioorg. Med. Chem. Lett.* **2006**, *16*, 5212–5216.

(54) Borhan, B.; Mebrahtu, T.; Nazarian, S.; Kurth, M. J.; Hammock, B. D. Improved radiolabeled substrates for soluble epoxide hydrolase. *Anal. Biochem.* **1995**, *231*, 188–200.

(55) Jones, P. D.; Wolf, N. M.; Morisseau, C.; Whetstone, P.; Hock, B.; Hammock, B. D. Fluorescent substrates for soluble epoxide hydrolase and application to inhibition studies. *Anal. Biochem.* **2005**, *343*, 66–75.

(56) Matveeva, E. G.; Morisseau, C.; Goodrow, M. H.; Mullin, C.; Hammock, B. D. Tryptophan Fluorescence Quenching by Enzyme Inhibitors As a Tool for Enzyme Active Site Structure Investigation: Epoxide Hydrolase. *Curr. Pharm. Biotechnol.* **2009**, *10*, 589–599.

(57) Schebb, N. H.; Huby, M.; Morisseau, C.; Hwang, S. H.; Hammock, B. D. Development of an online SPE-LC-MS-based assay using endogenous substrate for investigation of soluble epoxide hydrolase (sEH) inhibitors. *Anal. Bioanal. Chem.* **2011**, *400*, 1359–1366.

(58) Wolf, N. M.; Morisseau, C.; Jones, P. D.; Hock, B.; Hammock, B. D. Development of a high-throughput screen for soluble epoxide hydrolase inhibition. *Anal. Biochem.* **2006**, *355*, 71–80.

(59) Otwinowski, Z.; Minor, W. Processing of X-ray diffraction data collected in oscillation mode. *Macromol. Crystallogr., Part A* **1997**, *276*, 307–326.

(60) Winter, G. xia2: an expert system for macromolecular crystallography data reduction. *J. Appl. Crystallogr.* **2010**, *43*, 186–190.

(61) Bailey, S. The CCP4 Suite—programs for Protein Crystallography. *Acta Crystallogr., Sect. D: Biol. Crystallogr.* **1994**, *50*, 760–763.

(62) Painter, J.; Merritt, E. A. TLSMD web server for the generation of multi-group TLS models. *J. Appl. Crystallogr.* **2006**, *39*, 109–111.

(63) Emsley, P.; Lohkamp, B.; Scott, W. G.; Cowtan, K. Features and development of Coot. *Acta Crystallogr., Sect. D: Biol. Crystallogr.* **2010**, *66*, 486–501.

(64) Aley, K. O.; Levine, J. D. Rapid onset pain induced by intravenous streptozotocin in the rat. *J. Pain* **2001**, *2*, 146–150.